Criterion Delineating the Mode of Headcut Migration

By O. R. Stein,[1] Associate Member, ASCE, and P. Y. Julien,[2] Member, ASCE

Abstract: Two modes of headcut migration are generally recognized: (1) Rotating headcuts that tend to flatten as they migrate; and (2) stepped headcuts that tend to retain nearly vertical faces. A mathematical description of the sediment detachment potential immediately upstream and downstream of the headcut is used to delineate these modes of migration. The delineating parameter is the ratio of the time required to erode the headcut face from above to the time required to undermine the headcut face from below. This erosional time-scale ratio is a dimensionless function of flow, sediment, and geometry parameters. For the limiting case of homogeneous cohesive soils, the time-scale ratio is a simple function of a Froude number and the aspect ratio of drop height to normal flow depth. This relationship is calibrated using original laboratory experiments of headcut migration in initially vertical headcuts and verified by independent field experiments of headcuts propagating in four different homogeneous cohesive soils.

Introduction

A headcut is a natural, nearly vertical drop in channel bed elevation. The dissipation of flow kinetic energy at the drop causes excessive erosion and results in headcut upstream migration, which deepens and tends to widen the channel. Headcuts migrating in gullies may undermine upstream structures and, on a smaller scale, often define the breakpoint between overland and channel flow, and therefore play an important role in drainage network evolution. Headcuts propagating in small channels called rills contribute significantly to total upland soil losses due to erosive storms (Nearing et al. 1989). Several investigations (Blong 1970; 1985; Egboka and Okpoko 1984; Piest et al. 1975; Patton and Schumm 1975; Daniels and Jordan 1966; Kohl 1988) have focused on headcut migration in the field. Most data were collected after erosive storms and indicated that a nearly vertical face is maintained; however, information on the flow characteristics representing headcut migration was not reported. Therefore, understanding of the physical processes governing the formation, propagation, and degradation of headcuts as they migrate is very limited.

Several laboratory flume studies have observed headcut migration in specific bed materials. A knickpoint, which is a headcut in noncohesive sand, becomes indistinguishable from the rest of the channel as it propagates upstream, as shown by Brush and Wolman (1960). The data of Leopold et al. (1964) reveal the same result for cohesive soil, provided that the ratio of initial headcut drop height to flow depth in subcritical flow is less than one. Using stratified cohesive and noncohesive bed material, Holland and Pickup (1976) defined two headcut migration modes: (1) Rotating headcuts

[1]Asst. Prof., Dept. of Civ. and Agric. Engrg., Montana State Univ., Bozeman, MT 59717.

[2]Assoc. Prof., Dept. of Civ. Engrg., Colorado State Univ., Fort Collins, CO 80523.

Note. Discussion open until June 1, 1993. To extend the closing date one month, a written request must be filed with the ASCE Manager of Journals. The manuscript for this paper was submitted for review and possible publication on August 20, 1992. This paper is part of the ***Journal of Hydraulic Engineering***, Vol. 119, No. 1, January, 1993. ©ASCE, ISSN 0733-9429/93/0001-0037/$1.00 + $.15 per page. Paper No. 1888.

that alter their shape through migration, i.e., the Brush and Wolman (1960) observations; and (2) stepped headcuts that tend to maintain a nearly vertical face, i.e., the majority of field observations. Gardner (1983) reports similar observations and provides an excellent summary of geomorphological theories on headcut advancement.

The aim of this paper is to develop and test a criterion that separates stepped headcuts from rotating headcuts. The criterion was derived from the analysis of the erosion processes immediately upstream and downstream from a headcut. The criterion was tested with laboratory and field experiments of headcut migration, given steady uniform flow over a preexisting headcut geometry.

The approach used was to examine the changes in flow and sediment transport characteristics in the vicinity of the headcut. Flow upstream from the headcut was treated as an approach to a free overfall and flow downstream was examined as an impinging jet. Both flow conditions increase the applied bed shear stress, and erosion is calculated from a sediment detachment function based on excess shear stress. A headcut tends to migrate in a rotating mode if upstream erosion dominates, and a stepped mode if downstream erosion dominates. A criterion separating these modes of migration, defined as the ratio of upstream and downstream erosion time scales is tested with original laboratory experiments and independent field observations for the case of homogeneous cohesive soils.

Flow Characteristics

Two-dimensional flow over a headcut of drop height D_h in a wide rectangular channel of constant slope S is illustrated in Fig. 1. Steady flow of unit discharge q is uniform at a normal flow depth h_n and has a nearly hydrostatic pressure distribution upstream from the headcut. The pressure distribution is less than hydrostatic at the brink, causing the flow to accelerate through a distance L, approximately equal to two to four times h_n, upstream from the headcut. In this accelerated flow region, the depth gradually decreases from the normal flow depth h_n to a depth h_u at the brink, where the average flow velocity is V_u. It is considered that the water falls freely through a drop height D_h and accelerates from V_u at the brink to V_o when entering the impingement region. The jet impinges on the downstream water surface at a distance X_n downstream from the headcut face. At some distance downstream from the brink, the flow has been completely restored to normal depth.

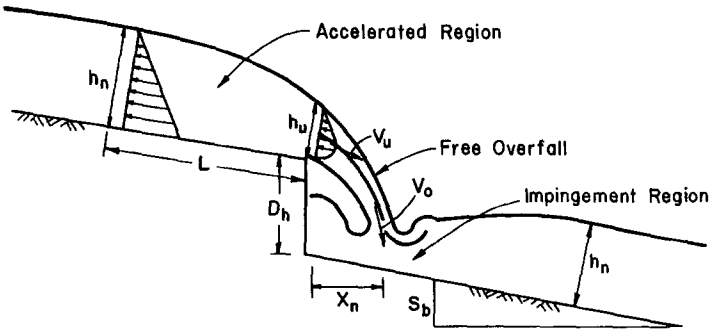

FIG. 1. Initial Headcut Hydraulics

Accelerated-Flow Region

The upstream normal flow depth h_n, and the corresponding normal flow velocity $V_n = q/h_n$, can be written as a power function of slope S and flow Reynolds number R (Julien and Simons 1985)

$$h_n = aS^b\mathrm{R}^c \quad \ldots\ldots (1)$$

in which the values of the coefficients a, b, and c are listed in Table 1. Hager (1983) and Hager and Hutter (1984) proposed an energy equation to determine changes in pressure and flow depth through the accelerated flow region. The following equation for both flow depth h_u and velocity V_u at the brink compares favorably with data from previous studies (Rouse 1936, 1937; Delleur et al. 1956; Rajaratnam and Muralidhar 1968):

$$\frac{V_n}{V_u} = \frac{h_u}{h_n} = \frac{\mathrm{F}^2}{\mathrm{F}^2 + 0.4} \quad \ldots\ldots (2)$$

in which F = upstream Froude number; h_u = flow depth at the brink; and V_u = velocity at the brink. The shear stress at the brink $\tau_u = C_u\rho V_u^2$ is compared to the normal shear stress $\tau_n = C_u\rho V_n^2$ in (3). Assuming that the upstream friction coefficient C_u remains constant, and using (2), one obtains

$$\frac{\tau_u}{\tau_n} = \frac{C_u\rho}{C_u\rho}\frac{V_u^2}{V_n^2} = \left(1 + \frac{0.4}{\mathrm{F}^2}\right)^2 \quad \ldots\ldots (3)$$

The shear stress at the brink τ_u is greater than the normal shear stress τ_n as given by the second term in parentheses of (3).

Free Overall Region

The free-falling nappe is accelerating from the brink to the impingement point. The velocity increases from V_u at the brink to V_o at the tailwater impingement point X_n. According to the equation of conservation of energy for free-falling fluid and assuming a small tailwater depth, the use of (2) yields

$$V_o = \sqrt{V_u^2 + 2gD_h} = V_n\left(1 + \frac{0.4}{\mathrm{F}^2}\right)\sqrt{1 + \frac{2gD_h}{V_u^2}} \quad \ldots\ldots (4)$$

and

TABLE 1. Summary of Flow Characteristics, Depth = $h_n = aS^b\mathrm{R}^c$

Type of flow (1)	a (2)	b (3)	c (4)
Laminar (k = constant)	$(k\nu^2/8g)^{1/3}$	−1/3	1/3
Turbulent, smooth boundary	$(0.22\nu^2/8g)^{1/3}$	−1/3	7/12
Turbulent (n = constant)	$(n\nu)^{6/10}$	−3/10	6/10
Turbulent (f = constant)	$(f\nu^2/8g)^{1/3}$	−1/3	2/3

$$\frac{X_n}{D_h} = V_u \sqrt{\frac{2}{gD_h}} = \sqrt{2} \sqrt{\frac{h_n}{D_h}} \left(\frac{F^2 + 0.4}{F} \right) \quad \ldots\ldots\ldots\ldots\ldots\ldots\ldots\ldots (5)$$

The two parameters V_o and X_n determine the velocity and location of the impact point of the jet entering the impinging region.

Impingement Region

Flow in the impingement region can be likened to that of an impinging plane jet. A general flow diagram for a jet produced by a free-falling nappe entering a plunge pool is shown in Fig. 2. At impact with the water surface, the jet has an initial thickness y_o, average velocity V_o, and impact angle χ. For some distance along the jet centerline, which defines the length of the potential core, diffusion has not affected velocity and the maximum velocity remains V_o. Beyond this potential core the maximum velocity is reduced by diffusion. Diffusion of an impinging turbulent jet and its interaction with impervious boundaries have been described by Beltaos and Rajaratnam (1973) and Beltaos (1974, 1976) and with porous boundaries by Kobus et al. (1979) and Bormann and Julien (1991).

Details of the relation between the diffusing jet below a headcut and scour hole development with time are given by Stein (1990) and Stein et al. (in press 1993). In summary, the maximum shear stress acting on the bed is in the vicinity of the intersection between the jet centerline and the bed, and is a function of the maximum velocity near the bed. The maximum bed shear stress in the impingement region occurs while the bed is within the jet potential core in which the maximum velocity remains V_o; therefore the maximum shear stress in the impingement region can be expressed as $\tau_d = C_d \rho V_o^2$.

The ratio of the maximum downstream shear stress to the normal shear stress is obtained from (2) and (4)

$$\frac{\tau_d}{\tau_n} = \frac{C_d \rho V_o^2}{C_u \rho V_n^2} = \frac{C_d}{C_u} \left[\left(1 + \frac{0.4}{F^2} \right)^2 + \left(\frac{2}{F^2} \frac{D_h}{h_n} \right) \right] \quad \ldots\ldots\ldots\ldots\ldots\ldots (6)$$

The shear stress ratio τ_d/τ_u is then given from the ratio of (6) and (3)

$$\frac{\tau_d}{\tau_u} = \frac{C_d}{C_u} \left[1 + \frac{2D_h}{h_n} \left(\frac{F}{F^2 + 0.4} \right)^2 \right] \quad \ldots\ldots\ldots\ldots\ldots\ldots\ldots\ldots\ldots\ldots (7)$$

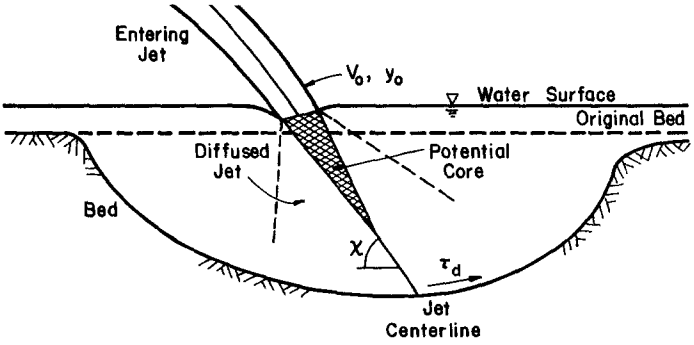

FIG. 2. Hydraulics of Impingement Region

This ratio is always larger than unity when $C_d \geq C_u$, which indicates greater shear stress at the jet impingement point than at the brink of the headcut.

Headcut Migration Mode

Rotating and stepped headcuts depend on the relative erosion rate in the accelerated and impingement regions. As illustrated in Fig. 3, the morphology of rotating and stepped headcuts depends on the time scales T_u and T_d of upstream and downstream scour. The upstream time scale T_u denotes the time for upstream vertical scour to reach the toe of the vertical face. Likewise, the downstream time scale T_d denotes the time for the impingement scour to develop horizontally and reach the toe of the vertical face. It is hypothesized that the ratio T_u/T_d can be used to delineate the mode of headcut migration. Conceptually, rotating headcuts would be obtained if $T_u < T_d$ or $T_u/T_d < 1$ if upstream erosion is dominant. Similarly, stepped headcuts would be maintained as $T_u > T_d$ or $T_u/T_d > 1$ if downstream erosion is dominant.

The time scales can be related to geometry and soil erosion characteristics. As given by Foster and Meyer (1975), the detachment rate of sediment particles per unit area E (in units of M/L^2T) depends on the applied shear stress τ exceeding the critical shear stress τ_c as

$$E = \kappa(\tau - \tau_c)^{\xi} = \kappa \left[\tau \left(1 - \frac{\tau_c}{\tau} \right) \right]^{\xi} \quad \ldots\ldots\ldots\ldots\ldots\ldots\ldots\ldots\ldots\ldots (8)$$

in which κ and ξ = empirical coefficients. Sediment detachment from the bed is also directly proportional to the bulk density of the soil B (in units of M/L^3) and the time change in bed elevation y; therefore $E_u = B_u(\partial y/\partial t)$. Integrating this expression from $y = 0$ at $t = 0$ to $y = D_h$ at $t = T_u$

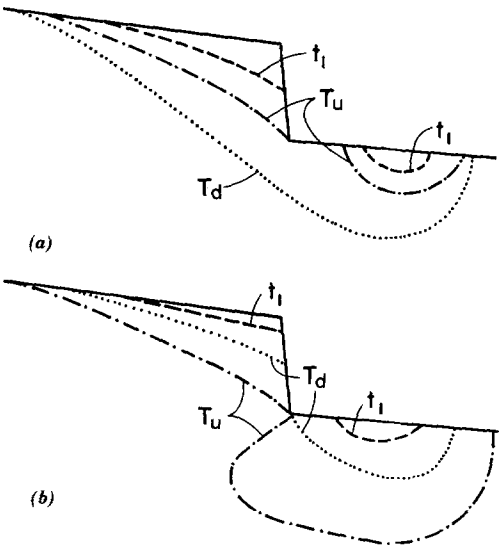

FIG. 3. Sketches of Headcut Migration: (*a*) Rotating Headcut $T_u < T_d$; and (*b*) Stepped Headcut $T_u > T_d$

yields the upstream sediment detachment $E_u = A_u B_u D_h / T_u$ in which A_u is an empirical coefficient and the subscript u denotes upstream conditions. Substituting this relation into (8) yields an expression for the upstream time scale T_u

$$T_u = \frac{A_u B_u D_h}{\kappa_u \tau_u^{\xi_u} \left(1 - \frac{\tau_{cu}}{\tau_u}\right)^{\xi_u}} \quad \ldots\ldots (9)$$

Similarly, the downstream time scale T_d is defined as the time required for downstream erosion to reach the headcut face. The corresponding length scale is the scour-hole half-length X_n between the headcut face and the initial point of jet impingement. Sediment detachment at the point of maximum scour can be expressed as $E_d = B_d(\partial D/\partial t)$, in which D is the maximum scour hole depth at any given time. Similarity of scour hole geometry, particularly in terms of length-depth ratio, has been observed by Stein (1990), Chee and Kung (1971), Rajaratnam (1981), Blaisdell et al. (1981) and Blaisdell and Anderson (1988a, b). Accordingly, integration from $t = 0$ to $t = T_d$ yields $E_d = A_d B_d X_n / T_d$, in which A_d is an empirical coefficient and subscript d denotes downstream conditions. Thus, the downstream time scale is

$$T_d = \frac{A_d B_d X_n}{\kappa_d \tau_d^{\xi_d} \left(1 - \frac{\tau_{cd}}{\tau_d}\right)^{\xi_d}} \quad \ldots\ldots (10)$$

Solving the upstream and downstream sediment detachment relationships, the ratio T_u/T_d obtained from combining (9) and (10) is

$$\frac{T_u}{T_d} = \frac{A_u B_u D_h \kappa_d \tau_d^{\xi_d} \left(1 - \frac{\tau_{cd}}{\tau_d}\right)^{\xi_d}}{A_d B_d X_n \kappa_u \tau_u^{\xi_u} \left(1 - \frac{\tau_{cu}}{\tau_u}\right)^{\xi_u}} \quad \ldots\ldots (11)$$

This equation, based on sediment detachment principles and headcut erosion time and length scales, constitutes a general physically based time

TABLE 2. Summary of Laboratory Experiments (Stein 1990)

Run (1)	q ($m^3/s \cdot m$) (2)	D_h (mm) (3)	S (4)	h_n (mm) (5)	D_h/h_n (6)	Froude number (7)	Calculated T_u/T_d (8)	Observed result (9)
28	0.00313	40	0.023	4.45	9.0	2.40	0.89	Uncertain
30	0.00127	10	0.059	1.92	5.2	3.43	0.24	Rotating
31	0.00142	10	0.018	3.04	3.3	1.92	0.43	Rotating
32	0.00142	40	0.018	3.04	13.1	1.92	2.37	Stepped
33	0.00266	40	0.014	4.77	8.4	1.83	1.44	Stepped
34	0.00414	60	0.014	6.18	9.7	1.94	1.55	Stepped
35	0.00267	60	0.027	3.84	15.6	2.55	1.57	Stepped
36	0.00266	20	0.027	3.83	5.2	2.55	0.42	Rotating
37	0.00417	40	0.027	4.98	8.0	2.69	0.61	Rotating
38	0.00269	40	0.027	3.86	10.4	2.54	0.94	Uncertain
39	0.00415	40	0.040	4.36	9.2	3.28	0.47	Rotating
40	0.00339	40	0.014	5.50	7.3	1.89	1.12	Uncertain

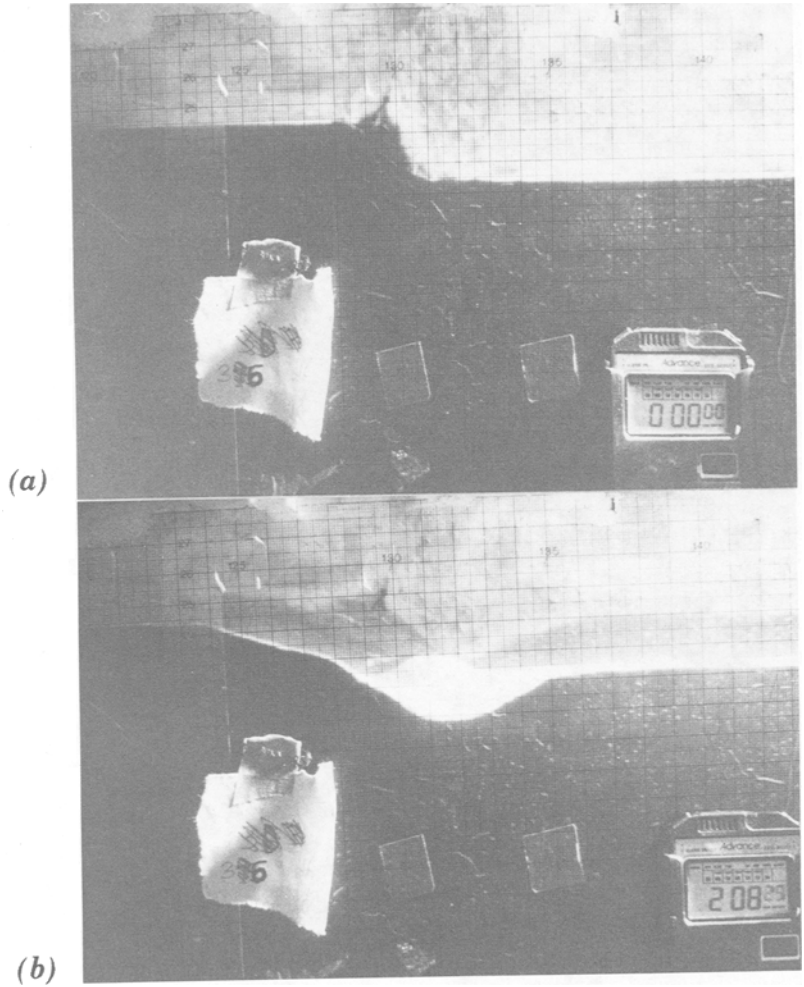

FIG. 4. Photographs of Typical Rotating Headcut

scale ratio describing the mode of headcut migration. It can be used to explain qualitative observations when sediments control headcut migration. For example, if the downstream soil is more erodible ($\tau_{cd} < \tau_{cu}$, $\kappa_d > \kappa_u$, or $\xi_d > \xi_u$) as in the case of stratified sediments, or if a surface compaction zone exists ($B_u > B_d$), the time-scale ratio is greater than one and the headcut tends to migrate in a stepped mode. However, in the particular case of homogeneous soils, in which $\tau_{cu} = \tau_{cd}$, $B_u = B_d$, $\kappa_u = \kappa_d = \kappa$, and $\xi_u = \xi_d = \xi$, and when the applied shear stress greatly exceeds the critical shear stress $\tau_u >> \tau_{cu}$ and $\tau_d >> \tau_{cd}$, so that both terms in parentheses in (11) approach unity, headcut migration becomes a function of hydraulics and geometry only. This is a limiting case, where clear cut differences in soil properties cannot explain headcut migration. After substituting (5) and (7) into (11) with the aforementioned assumptions, one obtains

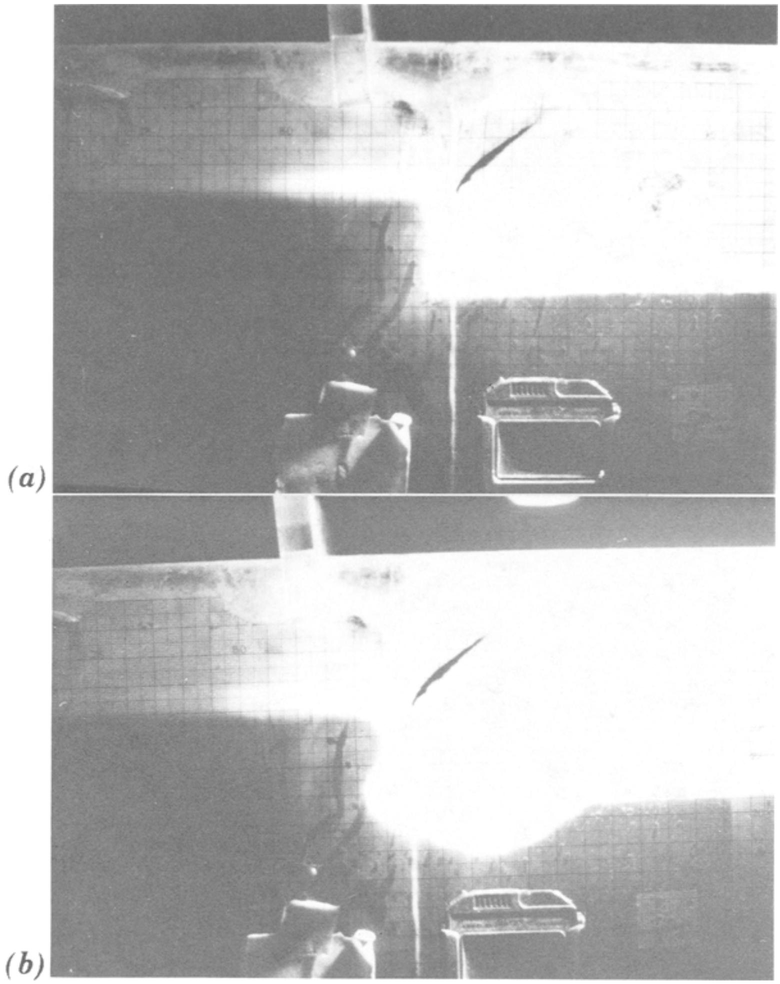

FIG. 5. Photographs of Typical Stepped Headcut

$$\frac{T_u}{T_d} \cong \frac{\Phi}{\Omega}[1 + \Phi^2]^{\xi} \qquad (12)$$

in which

$$\Phi = \sqrt{2}\sqrt{\frac{D_h}{h_n}}\left(\frac{\mathsf{F}}{\mathsf{F}^2 + 0.4}\right) \qquad (13a)$$

$$\Omega = 2\frac{A_d}{A_u}\left(\frac{C_u}{C_d}\right)^{\xi} \qquad (13b)$$

The separation between rotating and stepped headcuts is obtained from (12) when $T_u = T_d$, thus

TABLE 3. Summary of Field Experiments (Kohl 1988; Elliot et al. 1989)

Run (1)	q ($m^3/s \cdot m$) (2)	D_h (mm) (3)	S (4)	h_n (mm) (5)	D_h/h_n (6)	Froude number (7)	Calculated T_u/T_d (8)	Observed result (9)
Pal6R2	0.0298	27	0.059	6.35	4.3	1.18	1.29	Stepped
Pie22	0.0113	78	0.066	5.85	13.3	0.71	10.23	Stepped
Pie3R0	0.0103	30	0.071	5.80	5.2	0.62	2.74	Stepped
Pie3R4	0.0351	55	0.071	8.60	6.4	1.14	2.36	Stepped
Pie310	0.0405	24	0.071	13.05	1.8	0.79	0.68	Uncertain
Sve2R2	0.0315	33	0.045	4.80	6.9	1.33	2.02	Stepped
Sve22	0.0197	28	0.045	4.70	6.0	0.93	2.73	Stepped
Sve3R4	0.0457	32	0.046	6.55	4.9	1.30	1.34	Stepped
Sve32	0.0248	23	0.046	4.15	5.5	1.23	1.73	Stepped
Sve36	0.0525	50	0.046	5.90	8.5	1.46	2.28	Stepped
Sve6R2	0.0317	68	0.038	4.85	14.0	1.51	4.26	Stepped
Sve62	0.0144	25	0.038	5.15	4.9	0.80	2.34	Stepped
Bar22	0.0123	38	0.086	6.60	5.7	0.78	2.93	Stepped
Bar3R2	0.0234	29	0.089	7.25	4.0	1.01	1.47	Stepped
Bar6R0	0.0087	42	0.077	5.25	8.0	0.37	3.37	Stepped

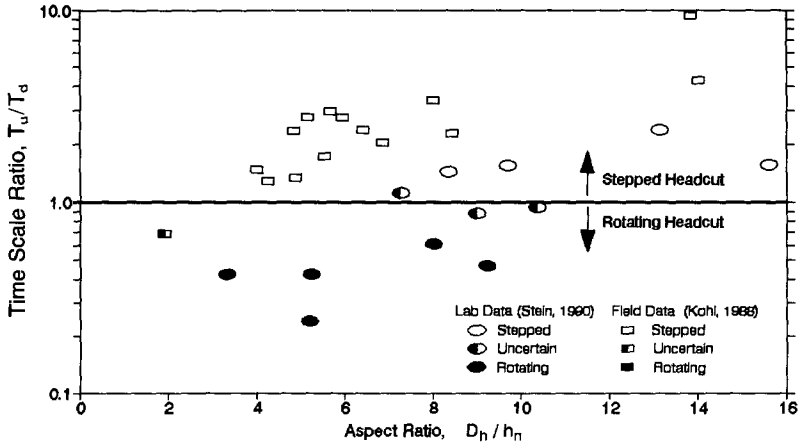

FIG. 6. Headcut Migration Criterion T_u/T_d versus Aspect Ratio

$$\Phi_c(1 + \Phi_c^2)^{\xi} = \Omega \quad \ldots\ldots (14)$$

in which Φ_c = critical value of Φ when the headcut is at the threshold between rotating and stepped migration. Separation lines between rotating and stepped headcuts can also be obtained by plotting the aspect ratio $\Psi = (D_n/h_n)$ versus the Froude number. The critical value of the aspect ratio $\Psi_c = D_h/h_n|_c$ determined from (12), (13), and (14) is

$$\Psi_c = \frac{\Phi_c^2}{2}\left(\frac{F^2 + 0.4}{F}\right)^2 \quad \ldots\ldots (15)$$

EXPERIMENTS

The headcut migration formulations of (12)–(15), applicable for the case of homogeneous cohesive soil, were calibrated using the experimental laboratory data of Stein (1990) and tested using field data on soil erodibility and headcut migration as reported by Kohl (1988) and Elliot et al. (1989).

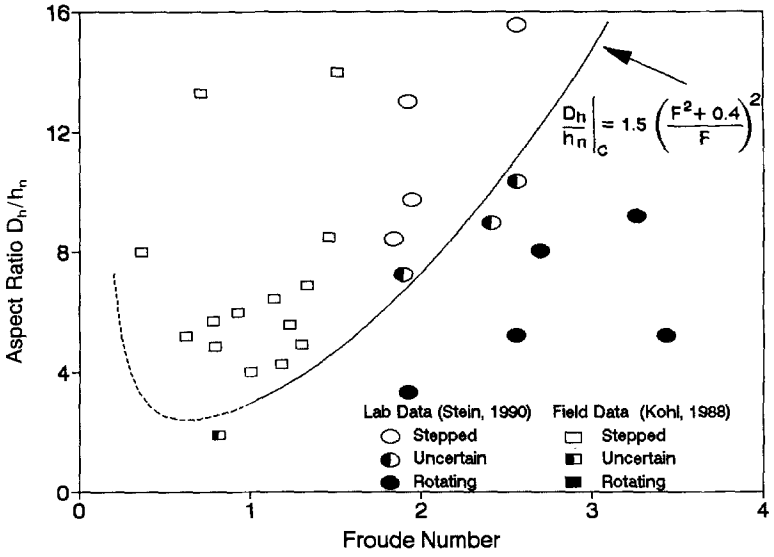

FIG. 7. Headcut Migration Criterion D_h/h_n versus Froude Number

Laboratory Experiments

A flume 10.4 cm wide and 2 m long was used for all laboratory experiments, and the bed material was a natural soil (Norka series collected in Colorado) susceptible to rill erosion and headcuts. A particle size analysis indicated the soil was 46.3% sand, 27.5% silt, and 26.2% clay with a mean particle size of $d_{50} = 0.046$ mm. To maintain uniform cohesive soil conditions and remove large pieces of organic matter, the air-dried soil was passed through a 0.420-mm sieve that destroyed large aggregates, but allowed the soil to retain cohesive properties upon rewetting.

Known weights of soil were placed in the flume and leveled after settling by manually shaking the small flume. The volume of each layer thus placed was measured to determine bulk density. Because the soil was sieved finely, a very uniform and constant bulk density of 1,320 $\pm$ 10 kg/m^3 was achieved. The final test bed, which was 23.3 cm thick, was slowly saturated by applying successive head increments of 4–8 cm to a reservoir below the flume floor. The head of each increment was held constant from 3 to 12 h, and at least 48 h elapsed between the start of wetting and the beginning of a run sequence. The final pressure head was set equal to the soil surface elevation to ensure full saturation. As many runs as possible were conducted in one flume packing, after which the uneroded soil was removed, air-dried, and resieved for future use.

Each run corresponds to a unique combination of flow rate, bed slope, and drop height. The drop height was formed by removing a block of soil between a cross section within the flume and the flume exit. The upstream and downstream bed surfaces were vertically offset by the drop height and flat between the flume sidewalls. Each run was inititated immediately after headcut formation and the cohesive properties of the soil maintained a vertical face while saturated. For all runs, the width to depth ratio was at least 16:1, and flow and headcut migration were observed to have minimal variation in width—therefore conditions were essentially two-dimensional.

Headcut migration was measured by photographing the longitudinal bed profile changes through the flume sidewall, which was imprinted with an x-y grid.

A total of 12 runs listed in Table 2 provide the data required to determine the time-scale ratio in (12), as well as the observed result from these runs. Reynolds numbers varied from 907 to 2,979, slopes from 0.014 to 0.059, and drop heights from 10 to 60 mm. The headcut in run 28 migrated about 400 mm in approximately 15 min. Runs 30–40 were abbreviated runs terminated when either upstream or downstream erosion dominated. Fig. 4 illustrates typical laboratory observations of a rotating headcut where the upstream erosion time scale is shorter than the downstream time scale, and Fig. 5 exemplifies a stepped headcut where the downstream time scale is shorter. The mode of headcut migration was visually determined from experiments and compared with computed time-scale ratios from (12). The predicted time-scale ratios T_u/T_d calculated from (12) with a value of $\xi = 1$ and $\Omega = 6.9$ varied from 0.24 to 2.37. The corresponding value of Φ_c from (14) is $\Phi_c = 1.7$.

Field Experiments

As part of experiments conducted to calibrate a newly developed upland erosion model (Elliot et al. 1989), rills preformed in 33 different agricultural soils were eroded by applying flow with and without rainfall simulation. On most rills several headcuts freely developed, and their formation and migration distance were recorded by Kohl (1988). The large data set was reduced to 15 headcuts on four different soil types by considering rills that developed only one headcut greater than 1 cm high. The headcut morphology data of Kohl (1988) and the pertinent hydraulic data of Elliot et al. (1989) are summarized in Table 3. The first three letters in the run nomenclature represent the soil type; the next digit represents the rill number: an R represents the presence of rainfall; and the last digit represents the nominal applied flow rate in gallons per minute. Reported Reynolds numbers varied from 987 to 4,539, slopes from 0.038 to 0.089, and drop heights from 23 to 78 mm.

Results

The laboratory and field data contained in Tables 2 and 3 are graphically represented in Fig. 6 as a plot of the calculated value of T_u/T_d from (12) versus aspect ratio D_h/h_n. The time-scale ratio varies over nearly two orders of magnitude from 0.24 to 10.23, and the aspect ratio varies from 1.8 to 15.6. A time-scale ratio of unity effectively separates stepped headcuts from rotating headcuts, accepting a narrow range of uncertainty ($0.8 \lesssim T_u/T_d \lesssim 1.2$), i.e., when upstream and downstream erosion rates are nearly identical. Under these conditions a knickpoint with an approximately 1:1 slope may migrate for some distance upstream, as observed in run 28. Laboratory headcuts in runs with time-scale ratios of less than approximately 0.8 were observed to rotate as they migrated, and undercutting of the headcut face was observed for laboratory runs with time-scale ratios greater than approximately 1.2. The observed result occurred more rapidly the greater the magnitude between the computed time-scale ratio and unity. The data have also been plotted in terms of aspect ratio versus Froude number in Fig. 7. The curve from (15) with $\Phi_c = 1.7$ effectively separates rotating and stepped headcuts. With only one exception, the reported field observations of stable headcut migration plot in the stepped-mode range.

Conclusions

A general formulation for the mode of headcut migration compares upstream and downstream erosion time scales as given in (11). This formulation is developed from a consideration of upstream and downstream sediment detachment that can be related to headcut hydraulics, sediment parameters, and geometry. A time-scale ratio T_u/T_d greater than one tends to form stepped headcuts, and rotating headcuts tend to form when $T_u/T_d < 1$. The tendency is more pronounced the further the ratio is from unity. For homogeneous cohesive soils, this time-scale ratio is written as a function of the drop height, flow depth, and Froude number, as given in (12) and (13). Separation between rotating and stepped headcuts can be achieved by comparing aspect ratio (D_h/h_n) and Froude number, as given in (15). The experiments validate the use of (12) and (15) for delineating stepped and rotating headcuts in homogeneous cohesive soils (Figs. 6 and 7, respectively). A numerical value of $\Omega = 6.9$ properly delineates rotating from stepped headcuts for laboratory and field measurements.

Acknowledgments

This study was undertaken primarily at the U.S. Department of Agriculture–Hydro-Ecosystems Group in Fort Collins, Colo. and special appreciation goes to D. DeCoursey. Additional funding at the Center for Geosciences under grant No., ARO/DAAL 03-86-K-0175 and the Montana Agricultural Experiment Station (No. J-2651) is gratefully acknowledged. The writers wish to thank W. J. Elliot, G. R. Foster, and K. D. Kohl for their insight and suggestions for improvement on final drafts of this manuscript.

Appendix I. References

Beltaos, S. (1974). "Turbulent impinging jets," PhD dissertation, University of Alberta, Edmonton, Alberta, Canada.

Beltaos, S. (1976). "Oblique impingement of plane turbulent jets." *J. Hydr. Div.*, ASCE, 102(9), 1177–1192.

Beltaos, S., and Rajaratnam, N. (1973). "Plane turbulent impinging jets." *J. Hydr. Res.*, 11(1), 29–59.

Blaisdell, F. W., Anderson, C. L., and Hebaus, G. G. (1981). "Ultimate dimensions of local scour." *J. Hydr. Div.*, ASCE, 107(3), 327–337.

Blaisdell, F. W., and Anderson, C. L. (1988a). "A comprehensive generalized study of scour at cantilevered pipe outlets pt. 1." *J. Hydr. Res.*, 26(4), 357–376.

Blaisdell, F. W., and Anderson, C. L. (1988b). "A comprehensive generalized study of scour at cantilevered pipe outlets pt. 2." *J. Hydr. Res.*, 26(5), 509–524.

Blong, R. J. (1970). "The development of discontinuous gullies in a pumice catchment." *Am. J. Sci.*, 268(4), 369–383.

Blong, R. J. (1985). "Gully sidewall development in New South Wales Australia." *Soil erosion and conservation*, S. A. El-Swaify, W. C. Moldenhauer, and A. Lo, eds., Soil Conservation Soc. Am., Ankeny, Iowa, 574–584.

Bormann, N. E., and Julien, P. Y. (1991). "Scour downstream of grade control structures." *J. Hydr. Engrg.*, ASCE, 117(5), 579–584.

Brush, L. M. Jr., and Wolman, M. G. (1960). "Knickpoint behavior in noncohesive material: a laboratory study." *Geol. Soc. Am. Bull.*, 71(1), 59–73.

Chee, S. P., and Kung, T. (1971). "Stable profiles of plunge basins." *Water Res. Bull.* 7(2), 303–308.

Daniels, R. B., and Jordan, R. H. (1966). "Physiographic history and the soils, entrenched stream of systems and gullies Harrison County Iowa." *USDA Tech. Bull. 1348*, U.S. Dept. of Agric., Washington, D.C.

Delleur, J. W., Dooge, J. C. I., and Gent, K. W. (1956). "Influence of slope roughness on the free overfall." *J. Hydr. Div.*, ASCE, 82(4), 1038-30–1038-35.
Egboka, B. C. E., and Okpoko, E. I. (1984). "Gully erosion in the Agula-Nanka region of Anambra State, Nigeria." *Challenges in African hydrology and water resources, Pub. No. 144,* Int. Assoc. Hydro. Sci., Delft, The Netherlands, 335–347.
Elliot, W. J., Liebenow, A. N., Laflen, J. M., and Kohl, K. D. (1989). "A compendium of soil erodibility data from WEPP cropland soil field erodibility experiments 1987 and 1988." *USDA-ARS National Soil Erosion Research Lab. Rept. No. 3*, Purdue Univ., West Lafayette, Ind.
Foster, G. R., and Meyer, L. D. (1975). "Mathematical simulation of upland erosion using fundamental erosion mechanics." *Present and Prospective Technol. for Predicting Sediment Yields and Sources (Proc., 1972 Sediment Yield Workshop USDA-ARS, ARS-S40)*, U.S. Dept. of Agriculture Sedimentation Lab, Oxford, Miss. 190–207.
Gardner, T. W. (1983). "Experimental study of knickpoint and longitudinal profile evolution in cohesive, homogeneous material." *Geol. Soc. Am. Bull.*, 94(5), 664–672.
Hager, W. H. (1983). "Hydraulics of plane free overfall." *J. Hydr. Engrg.*, ASCE, 109(12), 1683–1697.
Hager, W. H. (1984). Errata to "Hydraulics of Plane Free Overfall." *J. Hydr. Engrg.*, ASCE, 110(12), 1687–1688.
Hager, W. H., and Hutter, K. (1984). "Approximate treatment of plane channel flow." *Acta Mechanica*, 51(1–2), 31–48.
Holland, W. N., and Pickup, G. (1976). "Flume study of knickpoint development in stratified sediment." *Geol. Soc. Am. Bull.*, 87(1), 76–82.
Julien, P. Y., and Simons, D. B. (1985). "Sediment transport capacity of overland flow." *Trans., American Society of Agricultural Engineers*, 28(3), 755–762.
Kobus, H., Liester, P., and Westrich, B. (1979) "Flow field and scouring effects of steady and pulsating jets impinging on a moveable bed." *J. Hydr. Res.*, 17(3), 175–192.
Kohl, K. D. (1988). "Mechanics of rill headcutting," PhD dissertation, Iowa State University, Ames, Iowa.
Leopold, L. D., Wolman, M. G., and Miller, J. P. (1964). *Fluvial processes in geomorphology*. W. H. Freeman and Co., San Francisco, Calif.
Nearing, M. A., Foster, G. R., Lane, L. J., and Finkner, S. C. (1989). "A processed-based soil erosion model for USDA water erosion prediction project technology." *Trans., American Society of Agricultural Engineers*, 32(5), 1587–1593.
Patton, P. C., and Schumm, S. A. (1975). "Gully erosion, northwestern Colorado: A threshold phenomenon." *Geology*, 3(2), 88–90.
Piest, R. F., Bradford, J. M., and Wyatt, G. M. (1975). "Soil erosion and sediment transport from gullies." *J. Hydr. Div.*, ASCE, 101(1), 65–80.
Rajaratnam, N. (1981). "Erosion by plane turbulent jets." *J. Hydr. Res.*, 19(4), 339–359.
Rajaratnam, N., and Muralidhar, D. (1968). "Characteristics of the rectangular free overfall." *J. Hydr. Res.*, 6(3), 233–258.
Rouse, H. (1936). "Discharge characteristics of the free overfall." *Civ. Engrg.*, ASCE, 6(4), 257–260.
Rouse, H. (1937). "Pressure distribution and acceleration at the free overfall." *Civ. Engrg.*, ASCE, 7(7), 518.
Stein, O. R. (1990). "Mechanics of headcut migration in rills," PHD dissertation. Colorado State University, Fort Collins, Colo.

APPENDIX II. NOTATION

The following symbols are used in this paper:

a, b, c = coefficient and exponents from Table 1;
A_d, A_u = empirical coefficients in detachment equation;

B = soil bulk density;
C = coefficient of friction;
D = maximum depth of jet scour at arbitrary time;
D_h = initial drop height of headcut;
d_{50} = mean sediment size;
E = detachment of sediment particles;
f = Darcy-Weisbach friction factor;
F = Froude number;
g = gravitational acceleration;
h = flow depth at general cross section;
h_n = normal flow depth;
h_u = flow depth at free overfall brink;
k = resistance parameter for laminar flow;
L = length of accelerated flow region;
n = Manning resistance coefficient;
q = unit flow discharge;
R = Reynolds number;
S = bed slope gradient;
T_d = time scale for downstream scour;
T_u = time scale for upstream scour;
t_1 = arbitrary time $<T_u$ and $<T_d$;
V_o = initial velocity of jet;
V_n = average normal flow velocity;
V_u = average flow velocity at brink;
X_n = longitudinal distance form brink to tailwater impingement;
y_o = jet thickness;
κ, ξ = constants of sediment detachment equation;
ν = fluid density;
ρ = fluid density;
τ = shear stress at general cross section;
τ_c = critical shear stress for erosion initiation;
τ_d = shear stress in impingement region;
τ_n = normal flow shear stress;
τ_u = shear stress at brink;
Φ = function of aspect ratio and Froude number;
Φ_c = critical value of Φ;
χ = angle of jet at tailwater impingement;
Ψ_c = ratio of drop height to normal flow depth at Φ_c; and
Ω = function of empirical coefficients.

Subscripts

d = downstream; and
u = upstream.